Publications of the Astronomical Society of the Pacific, 128:115005 (15pp), 2016 November doi:10.1088/1538-3873/128/969/115005

The Xinglong 2.16-m Telescope: Current Instruments and Scientific Projects

Zhou Fan[1], Huijuan Wang[1], Xiaojun Jiang[1], Hong Wu[1], Hongbin Li[1], Yang Huang[2], Dawei Xu[3], Zhongwen Hu[4], Yinan Zhu[1], Jianfeng Wang[1], Stefanie Komossa[5], and Xiaoming Zhang[1]

[1] Key Laboratory of Optical Astronomy, National Astronomical Observatories, Chinese Academy of Sciences, 20A Datun Road, Chaoyang District, Beijing 100012, China; zfan@bao.ac.cn

[2] Department of Astronomy, Peking University, Beijing 100871, China

[3] Key Laboratory of Space Astronomy and Technology, National Astronomical Observatories, Chinese Academy of Sciences, 20A Datun Road, Chaoyang District, Beijing 100012, China

[4] Nanjing Institute of Astronomical Optics & Technology, National Astronomical Observatories, Chinese Academy of Sciences, 188 Bancang Street, Nanjing 210042, China

[5] Max-Planck-Institut fuer Radioastronomie, Auf dem Huegel 69, D-53121 Bonn, Germany

Received 2016 January 12; accepted 2016 May 16; published 2016 October 4

Abstract

The Xinglong 2.16-m reflector is the first 2-m class astronomical telescope in China. It was jointly designed and built by the Nanjing Astronomical Instruments Factory (NAIF), Beijing Astronomical Observatory (now National Astronomical Observatories, Chinese Academy of Sciences, NAOC), and Institute of Automation, Chinese Academy of Sciences in 1989. It is a Ritchey-Chrétien (R-C) reflector on an English equatorial mount and the effective aperture is 2.16 m. It had been the largest optical telescope in China for ∼18 years until the Guoshoujing Telescope (also called Large Sky Area Multi-Object Fiber Spectroscopic Telescope, LAMOST) and the Lijiang 2.4-m telescope were built. At present, there are three main instruments on the Cassegrain focus available: the Beijing Faint Object Spectrograph and Camera (BFOSC) for direct imaging and low-resolution ($R \sim 500$–2000) spectroscopy, the spectrograph made by Optomechanics Research Inc. (OMR) for low-resolution spectroscopy (the spectral resolutions are similar to those of BFOSC) and the fiber-fed High Resolution Spectrograph (HRS; $R \sim 30{,}000$–$65{,}000$). The telescope is widely open to astronomers all over China as well as international astronomical observers. Each year there are more than 40 ongoing observing projects, including 6–8 key projects. Recently, some new techniques and instruments (e.g., astro-frequency comb calibration system, polarimeter, and adaptive optics) have been or will be tested on the telescope to extend its observing abilities.

Key words: instrumentation: miscellaneous – instrumentation: photometers – instrumentation: spectrographs – telescopes

Online material: color figures

1. Introduction

The 2.16-m reflector is an English equatorial mount telescope at Xinglong Observatory, and it obtained the first light in 1989, which was built/developed by the Chinese independently. The effective aperture of the telescope is 2.16 m, and the focal ratio of the primary mirror is f/3 (Su et al. 1989). The effective aperture of the secondary mirror is 0.717 m. Currently, there are two available foci for mounting astronomical observing instruments, the Cassegrain focus and the Coudé focus. For the Cassegrain focus, which is an R-C system, the focal ratio is f/9, and the scale on the focal plane is $10\farcs61\ \mathrm{mm}^{-1}$. While for the Coudé system, it is f/45, and the scale on the focal plane is $2\farcs12\ \mathrm{mm}^{-1}$. The most special character of the optical system is that the Cassegrain system and the Coudé system share the same secondary mirror and there is a relay mirror in the Coudé system, and both systems can sufficiently eliminate the spherical aberration and coma aberration (Su et al. 1989).

Since its first light in 1989, the 2.16-m telescope has been used in various scientific research fields in Galactic and extragalactic astrophysics, including the determination of stellar parameters (e.g., abundances, surface gravity, temperatures) of a large sample of stars, the discoveries of substellar and planetary companions of stars, studies of active galaxy nuclei (AGNs), including the identifications of high-redshift quasars, discoveries, and studies of supernovae, e.g., 1993J (Wang & Hu 1994), as well as time-domain science (e.g., supernovae, gamma-ray bursts, stellar tidal disruption events, and variable stars).

Although the 2.16-m telescope is the third largest optical telescope in China right now (smaller than LAMOST (Cui et al. 2012) and the Lijiang 2.4-m telescope (Fan et al. 2015), which were installed in 2008 and 2007, respectively), it plays an important role in Chinese astronomical observations. Every year there are hundreds of Chinese astronomers applying for observing time at the 2.16-m telescope, including significant

numbers of new telescope users and graduate students. Therefore, it is of great importance and useful to describe the specific parameters and the observing ability of the telescope and its instruments to the telescope users, which could be very helpful for planning and carrying out observations and for the data reduction. This paper is organized as follows: the Xinglong Observatory is introduced in Section 2; the telescope and its instruments are described in Section 3; and the efficiencies of the telescope and its instruments also have been estimated in this section. The relevant science and projects based on observational data obtained by the 2.16-m telescope are described in Section 4; finally, a brief summary is given and some future facilities are discussed in Section 6.

2. The Xinglong Observatory

The Xinglong Observatory of National Astronomical Observatories, CAS (NAOC; IAU code 327, coordinates: 40° 23′39″ N, 117°34′30″ E) was founded in 1968. At present, it is one of most primary observing stations of NAOC. As the largest optical astronomical observatory site in the continent of Asia, it harbors nine telescopes with an effective aperture greater than 50 cm. These are LAMOST, the 2.16-m reflector, a 1.26-m optical, and near-infrared reflector, a 1-m Alt-Az reflector, an 85-cm reflector (NAOC-Beijing Normal University Telescope, NBT), an 80-cm reflector (Tsinghua University-NAOC, TNT), a 60/90-cm Schmidt telescope, a 60 cm reflector, and a 50-cm reflector. The average altitude of the Xinglong Observatory is ∼960 m, and it is located at the south of the main peak of the Yanshan Mountains, in the Xinglong county, Hebei province, which is ∼120 km northeast of Beijing. The mean and median seeing values of the Xinglong Observatory are 2.″0 and 1.″8, respectively, and on average, there are 117 photometric nights and 230 useful nights per year based on the data of 2007–2014 (Zhang et al. 2015). For most of the time, the wind speed is less than 4 m s^{-1} (the mean value is 2 m s^{-1}), and the sky brightness is ∼21.1 mag $arcsec^2$ in the V band at the zenith (Zhang et al. 2015).

Each year, more than 100 astronomers use the telescopes of Xinglong Observatory to perform the observations for the studies on Galactic sciences (stellar parameters, extinction measurements, Galactic structures, exoplanets, etc.) and extragalactic sciences (including nearby galaxies, AGNs, high-redshift quasars), as well as time-domain astronomy (supernovae, gamma-ray bursts, stellar tidal disruption events, and different types of variable stars). In recent years, besides the basic daily maintenance of the telescopes, new techniques and methods have been explored by the engineers and technicians of Xinglong Observatory to improve the efficiency of observations. Meanwhile, the Xinglong Observatory is also a national popular-science and education base of China for training students from graduate schools, colleges, high schools, and other educational institutions throughout China, and it has hosted a number of international workshops and summer schools.

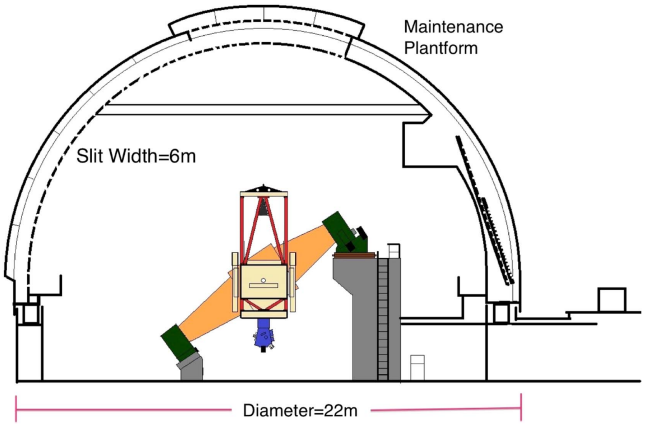

Figure 1. Illustration of the 2.16-m telescope at Xinglong Observatory, which is an English equatorial mount, in a large dome with a diameter of 22 m. (A color version of this figure is available in the online journal.)

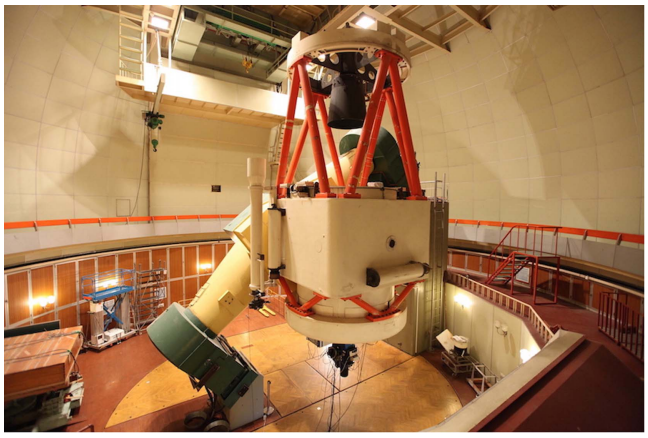

Figure 2. Xinglong 2.16-m telescope at Xinglong Observatory. (A color version of this figure is available in the online journal.)

3. The 2.16-m Reflector and Its Instruments

As shown in Figures 1 and 2, the telescope is an R-C system on an English equatorial mount. The effective aperture of the primary mirror is 2.16 m. Currently, there are three primary instruments available for the Cassegrain focus: BFOSC, OMR, and the fiber-fed HRS. Previously, a high-resolution spectrograph was mounted on the Coudé focus before the fiber-fed HRS was mounted in 2010. Since then, the Coudé focus has only been used for a few special experiments, such as adaptive optics tests. As shown in Figure 1, the diameter of the dome is 22 m, which is relative large for a 2-m-class telescope, due to its design. The rotation part of the telescope weighs 91 tons, and the pointing accuracy that is modified with the

pointing model is rms = 10.″0. While the tracking precision of the telescope is rms = 20.″0 within 10 minutes, and rms = 50.″0 within 1 hour. The position precision of the telescope on the sky under guiding is rms < 0.″15 (Huang et al. 2015).

3.1. The BFOSC Instrument

The BFOSC is one of the primary instruments of the telescope, for which the design and processing of mechanism and electronics control; the design of grims and assembling and debugging of the whole system were done by the University of Copenhagen, and ESO provided consult and optical design of the focal reducer. It is available for the f/9 Cassegrain focus. The scale of the focal plane is 10.″61 mm^{-1}. As discussed in Section 1, it can be used for both imaging mode and spectroscopy mode, which is switchable. Figure 3 shows the optical layout of the BFOSC instrument, including the aperture wheel, filter wheel, grism/echelle wheel, calibration device, guiding device, collimator, shutter, camera, and the CCD detector.

There are eight positions on the aperture wheel: three of them for direct imaging, coronagraph mask, and focal adjusting plate, respectively, and the other five for long/short slit plates. For the long slits, the lengths are all 9.′4, and there are nine options for the slit widths (0.″6, 0.″7, 1.″1, 1.″4, 1.″8, 2.″3, 3.″6, 7.″0, and 14.″0). While for the short slits, the slit lengths are various for different slit widths: 3.″5 for slit width of 0.″6, 4.″0 for slit width of 1.″0, 3.″6 for slit width of 1.″6, and 3.″7 for both slit widths of 2.″3 and 3.″2. The coronagraph mask is used to block out the intense light from bright sources near the observing targets, with circular spots of which the diameters are 2.″0, 3.″0, 4.″0, 6.″0, 9.″0, and 12.″0.

For the filter wheel, there are several sets of filters available. The Johnson-Cousins *UBVRI* filters are for the broadband photometry. In addition, there are special filters used for the spectroscopic observing: the *Z* band for the transmitting spectral region $\lambda \geqslant 910$ nm, and the 385*LP* band for removing the second-order spectrum in the wavelength region $\lambda \leqslant 385$ nm. The transmission curves are shown in Figure 4.

Besides, a series of interference narrowband filters covering [O III] (rest-frame wavelength of λ5007A), Hα, and He II(rest-frame wavelength λ4686A) is also available for the BFSOC imaging mode. For series of [O III] band observations, there are eight filters of which the central wavelengths are between 500.9 and 536.0 nm with FWHM of 6 nm, corresponding to redshifts of 0–20000 km s^{-1}. While for the series of H_α bands, there are 11 filters of which the central wavelengths are between 656.2 and 706.0 nm with an FWHM of 7 nm, corresponding to redshifts of 0–22000 km s^{-1}. For the He bands, there are three filters of which the central wavelengths are between 447.1 and 468.6 nm with an FWHM of 6 nm. In addition, an [O III] filter with an FWHM of 13 nm and an H_α filter with FWHM of 14 nm are also provided for a redshift of $z = 0$. These filters can be used for the study of star-forming regions of nearby galaxies at different redshifts.

Table 1 presents the parameters of the grisms/prisms/echelle for the BFOSC instrument. From left to right in the columns are names, working spectral orders, reciprocal linear dispersions, dispersions, and wavelength coverages of the various grisms/prisms/echelle, respectively. The configurations can be chosen by the users depending on the different requirements of the projects. For grisms G3/G6/G10, the blue ends of wavelength coverages are limited by the cutoff of the atmospheric window, while for grisms G5/G8, the red ends are limited by the size of the CCD. The low dispersion grisms G10/G11/G12 are also used for the cross-disperser when mounted on the filter wheel. The echelle E13 is only used for measuring the velocity field of extended sources with the third-order spectrum, and the *V* band filter is recommended to be applied together with it to remove the other order of the spectrum.

Table 2 presents the spectral resolutions of some frequently using BFSOC grisms at a minimum slit width 0.″6 and a slit width of ∼2.″3 used in typical seeing conditions, which are estimated with the emission lines of the planetary nebula (PN) IC4997. The observations were taken on 2014 November 24 and 2016 February 26, with gratings of G4, G6, G7, and G8 on BFOSC. Throughout the nights of the observations, the weather was clear, and the seeing was between ∼2.″0 and 2.″4. The exposure time was 0.2–10 s depending on the dispersions of the different grisms. The shortest exposure of 0.2 s is considerably longer than the shutter speed of 1.5 ms.

For the calibration device, four lamps can be mounted at most. One is for the flat-fielding correction, and the other lamps can be used for wavelength calibration. The lights of the lamps illuminate the integrating sphere at first, then are modified to be f/9 light beam, and finally are reflected to the focal plane of the BFOSC instrument. The Fe lamp and Ne lamp are frequently used for the wavelength calibration.

On the guiding device, a mirror reflects the view outside of the observing field of view (FOV) to an ICCD, which is movable in 3D directions to find a proper guide star and also to adjust the focus. The FOV of the guiding device is 10′ × 20′, which is large enough to find a suitable guide star.

In 2010, an E2V 55–30–1–348 back-illuminated CCD, AIMO, was installed on the spectrograph, and the CCD controller was made by the Lick Observatory. The size of the CCD is 1242 × 1152 pixels with a pixel size of 22.5 μm. The pixel scale is 0.″457, and the FOV is 9.′46 × 8.′77 according to the size of the CCD. Figure 5 shows the quantum efficiency (QE) of the CCD. It can be seen that the maximum QE is higher than 90% around 5700 Å of the wavelength.

Table 3 lists the gains, readout noises, and readout speed of the BFOSC CCD at various readout times. Observers can

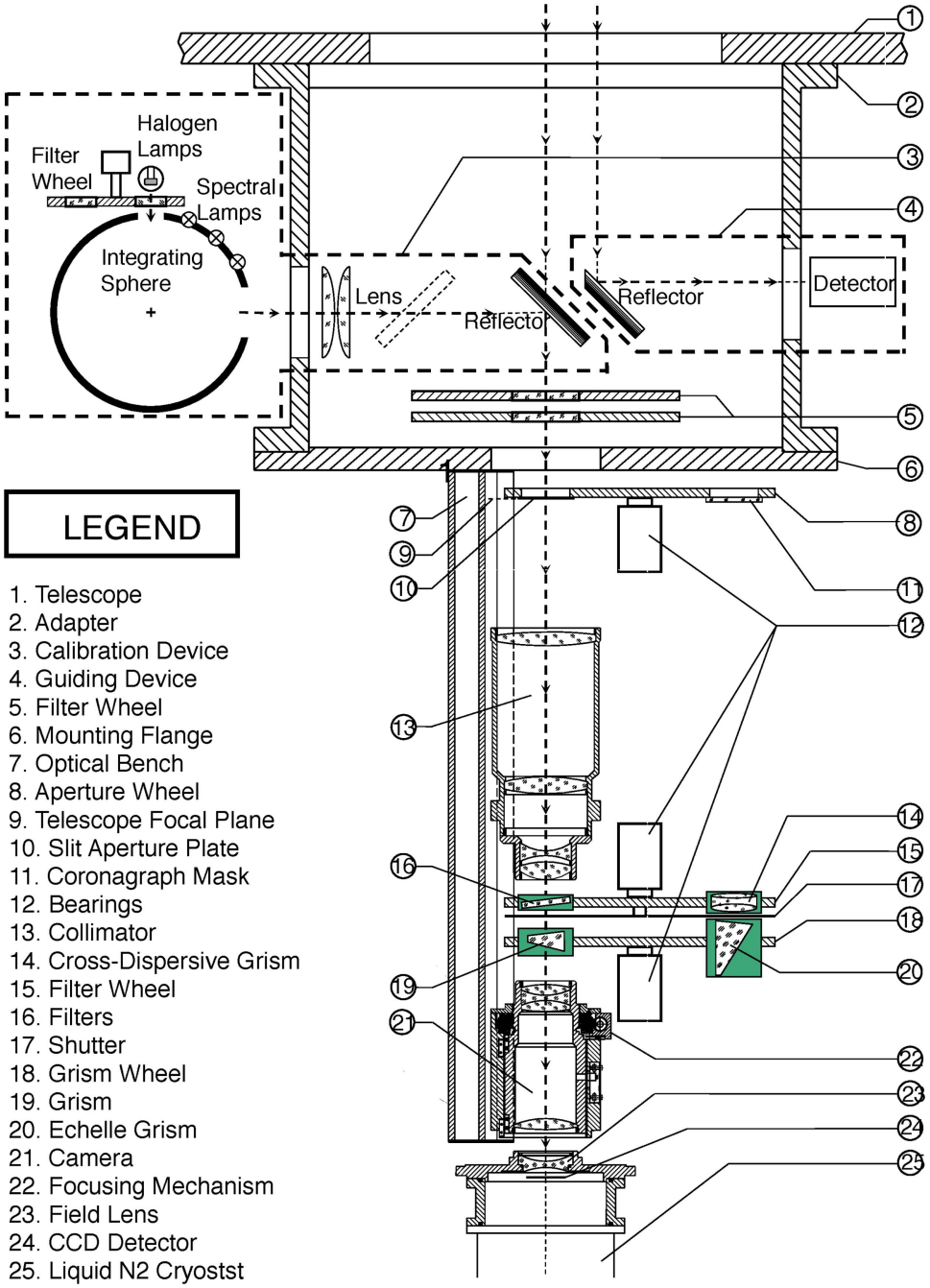

Figure 3. Optical and mechanical layout of the BFOSC instrument from Huang et al. (2012).
(A color version of this figure is available in the online journal.)

choose different options for the specific observations, and the slow readout speed is applied in most of the time.

There are six observing modes for the BFOSC instrument: (1) direct imaging, (2) long-slit spectroscopy, (3) slitless spectroscopy, (4) echelle grism spectroscopy, (5) coronograph mask, and (6) multiple-object spectroscopy. Figure 6 shows the optical layout of the lens and light path for the direct imaging mode and the spectroscopy observing mode, which could be switched in a few minutes.

Since 2012, a multi-object spectroscopy (MOS) observing mode of BFSOC is available for observers by placing a multiple-aperture mask on the aperture wheel (Zhou

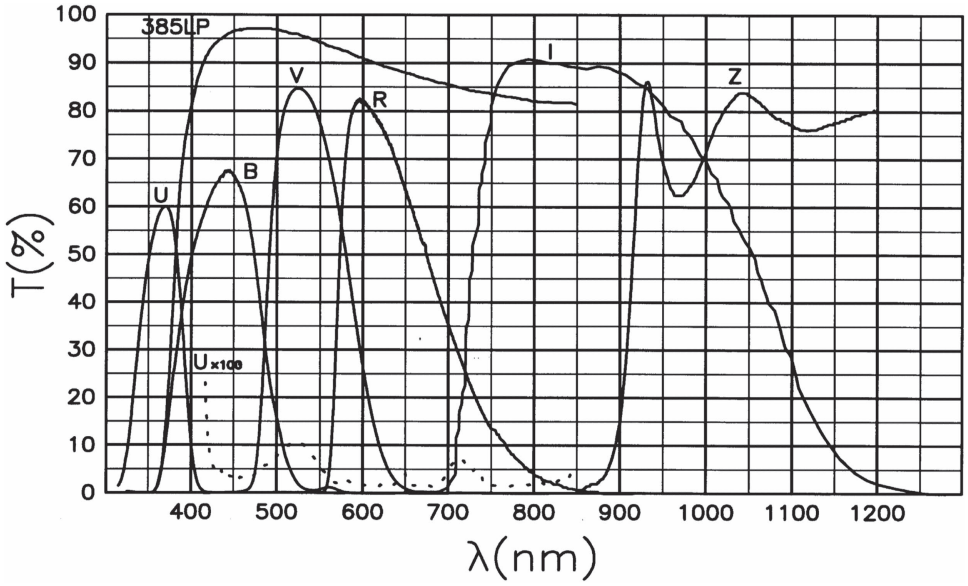

Figure 4. Transmission curves of the BFOSC filters, including the Johnson-Cousins *UBVRI* bands as well as the 385*LP* and *Z* bands for spectroscopic observations.

Table 1
The Parameters of Grisms/Prisms/Echelle for the BFOSC Instrument from Huang et al. (2012)

Name	Spec. Ord.	Rec. Lin. Disp. (Å mm^{-1})	Disp. (Å pix^{-1})	Wav. Range (Å)
P1		573–2547	8.6–38.2	4000–5600
G3	1	139	3.12	3300–6400
G4	1	198	4.45	3850–7000
G5	1	199	4.47	5200–10120
G6	1	88	1.98	3300–5450
G7	1	95	2.13	3870–6760
G8	1	80	1.79	5800–8280
G10	1	392	8.80	3300–6400
G11	1	295	6.63	3900–7300
G12	1	837	18.8	5200–10200
E9+G10	21–11	16.8–38.4	0.38–0.86	3300–6400
E9+G11	18–9	21.0–47.9	0.47–1.076	3900–7300
E9+G12	14–6	29.0–73.2	0.65–1.64	5200–10200
E13+V	3	33.1	0.75	4980–5990

et al. 2014). In this mode, 10–20 objects can be observed simultaneously, depending on the spatial distribution density of the targets. The MOS improves the observing efficiency of multiple-object observations, such as star-forming activities of H II regions of nearby galaxies, star clusters, or groups and clusters of galaxies.

Table 2
Spectral Resolutions of Several Frequently used Grisms of BFSOC at a Slit Width of 0.″6 and 2.″3, which is around the Typical Seeing

Wavelength	G4	G6	G7	G8	G4	G6	G7	G8
(Å)		0.″6				2.″3		
4341	531	1423	1204	…	246	463	478	…
4363	557	1503	1252	…	…	…	…	…
4861	…	…	…	…	262	538	521	…
4959					265	540	524	…
5007	620	1413	1328	…	265	555	532	…
6563	824	…	…	2245	321	…	…	820

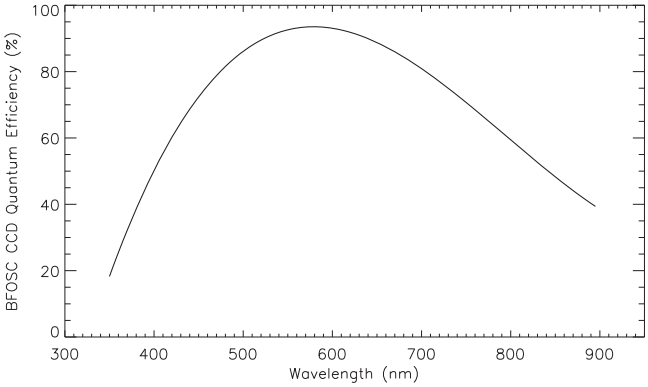

Figure 5. Quantum efficiency of the BFOSC CCD camera.

Table 3
Gains, Readout Noises, and Readout Speed of BFOSC CCD from Huang et al. (2012)

Readout Speed	Mode	Gain (e^- ADU^{-1})	Readout Noise (e^- pix^{-1})	Readout Time (second)
Fast	0	99.58	132.5	5
Fast	1	49.44	103.7	5
Fast	2	24.48	87.35	5
Median	0	2.33	6.80	8
Median	1	1.22	5.93	8
Median	2	0.50	6.06	8
Slow	0	2.43	3.25	28
Slow	1	1.13	2.58	28
Slow	2	0.50	2.46	28

The total efficiency of the observing system, including the atmosphere, telescope, and its instruments, is what the observers are mostly concerned about. In fact, there are a number of factors to be considered for calculating the total efficiency of the system, such as atmospheric extinction, reflectivity of primary and secondary mirror, transmissions of filters, and the quantum efficiency of the CCD. It can be estimated through observing standard stars in Equation (1):

$$\eta(\lambda) = \frac{F_{\rm ADU} \cdot G}{F_\lambda \cdot \delta\lambda \cdot S_{\rm tel}}. \quad (1)$$

In this formula, $F_{\rm ADU}$ is the observed number counts of a standard star per second (ADU s^{-1}), G is the gain of the CCD (e^{-1} ADU^{-1}), F_λ is theoretical photon flux of a standard star derived from its AB mag (photon s^{-1} cm^{-2} Å^{-1}), $\delta\lambda$ is the effective bandwidth of the filter in imaging observations or the dispersion of the grating for spectroscopic observations (Å), $S_{\rm tel}$ is the effective area of the primary mirror of the telescope (cm^2), and λ is the effective wavelength of the filter or the wavelength at which the efficiency is to be computed for the spectroscopy (Å).

In order to estimate the total efficiency of the 2.16-m telescope, a Landolt standard star PG2336+004B was observed on 2014 November 21 in the broadband *UBVRI* bands of the BFOSC photometric system by using Equation (1). The seeing was ~2.″0–3.″0 throughout the whole night of observations, and the airmass is ~1.3. Figure 7 is a plot of the total efficiency in different bands as a function of central wavelength. The atmospheric extinction, reflectivity of primary and secondary mirrors, transmissions of filters, QE of CCD, as well as other factors, were not corrected in the calculation. It can be seen that the total efficiency is relatively low in the *U* band (~2%) and *B* band (~7%), but it is relatively high in the *VRI* bands (~15%).

The limiting magnitude is also an important quantity to evaluate the observing ability of a telescope. Actually, at the same night on 2014 November 21, a Landolt standard star PG2336+004 was observed in the *UBVRI* bands. The airmass was ~1.3. The limiting magnitude (signal-to-noise ratio, S/N = 5) as a function of exposure time in the *UBVRI* bands are shown in Figure 8, and the same relations but for the limiting magnitudes of S/N = 10 are shown in Figure 9. It is noted that in the 640 s exposure the limiting magnitudes of the *B*/*V*/*R* bands could reach ~22 mag in S/N = 5 and ~21 mag in S/N = 10. The limiting magnitude in the *U* band is the lowest because the sensitivity of the observing system in the blue band is relatively low, further affected by the effect of significant atmospheric extinction in the blue band. However, although the efficiency in the *I* band is similar to those of the *VR* bands, the night-sky background is much brighter (~2 times) than in the *VR* bands. In addition, the fringe of the CCD in the *I* band contributes significant noise. Although we have tried the de-fringing method introduced by Chen et al. (1987), it has not been improved significantly. Therefore, these factors together make the limiting magnitudes ~1 mag shallower than those in the *BVR* bands.

In order to estimate the efficiency of the spectroscopic system of BFOSC, the two ESO standard stars HR153 and HR9087 were observed on 2014 November 24, with several frequently used grisms (G4, G5, G6, G7, and G8) of the BFOSC instrument. The weather was clear, and the seeing was ~2.″4. The exposure time was 0.2–10 s according to the dispersions of the grisms. To make sure that most of the flux can be obtained and measured for estimating the efficiency, the slit was configured as 7.″0. The total efficiency, which is defined above, including atmospheric extinction and instruments, was calculated with Equation (1) and shown in Figure 10. For the grisms G4 and G5, the peak efficiencies are ~15% and ~10%, respectively, while for the other three grisms, the total efficiencies of the peak are ~5%. The filter 385*LP* was used for removing the second-order spectrum of wavelength $\lambda \geqslant 385$ nm.

For the limiting magnitude in the spectroscopic observations, the previous observations show that typically it could reach $V = 20$ mag of S/N = 5 in the grism G6, with an exposure of 1 hour, given by Huang et al. (2012).

3.2. The Spectrograph Made by Optomechanics Research Inc. (OMR)

The OMR is another low-resolution spectrograph available on the Cassegrain focus of the 2.16-m telescope. It was made by Optomechanics Research Inc. (Arizona, USA) at the end of 1994 and was tested on the 2.1-m telescope at Kitt Peak. Then, it was installed on the 2.16-m telescope of Xinglong Observatory in 1995 and was available to astronomers in 1996.

The optical layout of the OMR is shown in Figure 11. The system is composed of slit and decker assembly, filters, spectrograph, calibration system, collimator, gratings, CCD camera, guiding CCD camera, console, and data-collecting system.

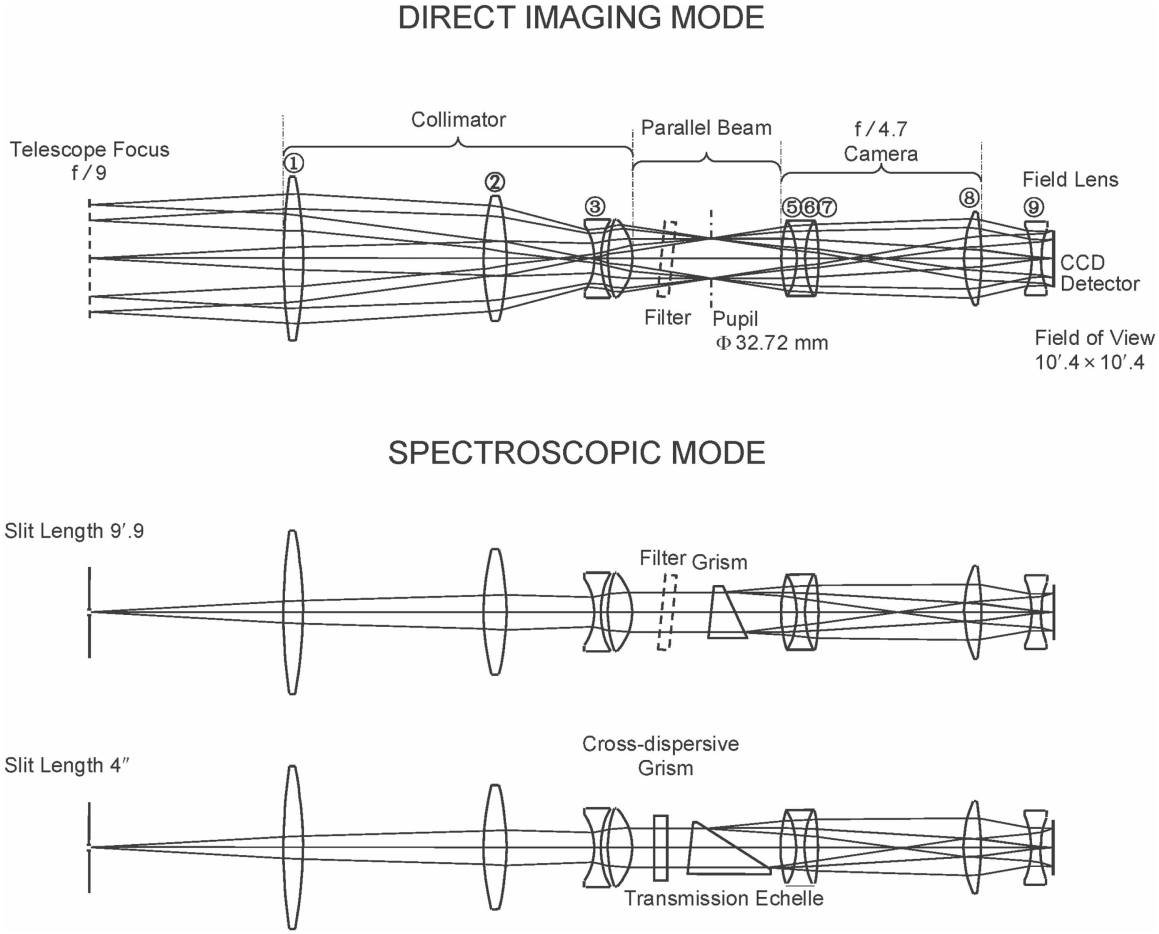

Figure 6. Layout of the lens of two different working modes of the BFOSC instrument from Huang et al. (2012).

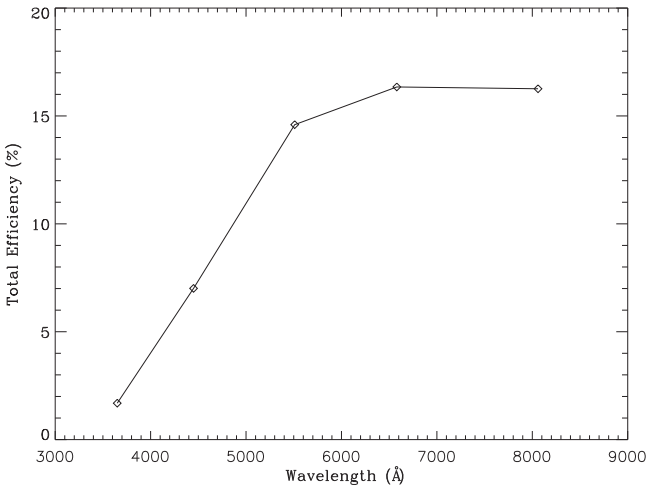

Figure 7. Total efficiency of the BFOSC photometric system including the atmosphere of the 2.16-m telescope in the *UBVRI* bands at an airmass of ∼1.3.

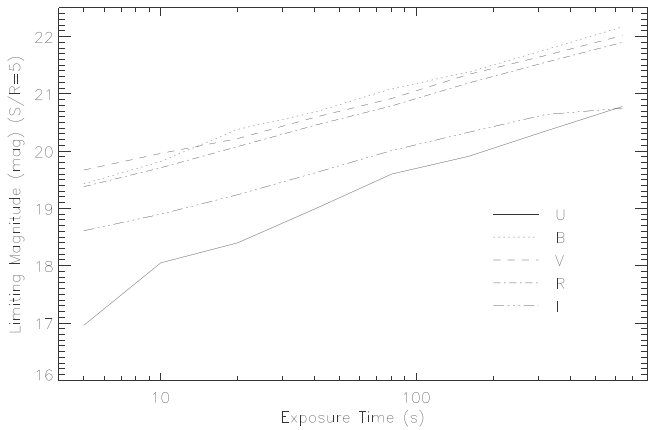

Figure 8. Limiting magnitudes in the *UBVRI* bands for the signal-to-noise ratio of S/N = 5 at an airmass of ∼1.3.

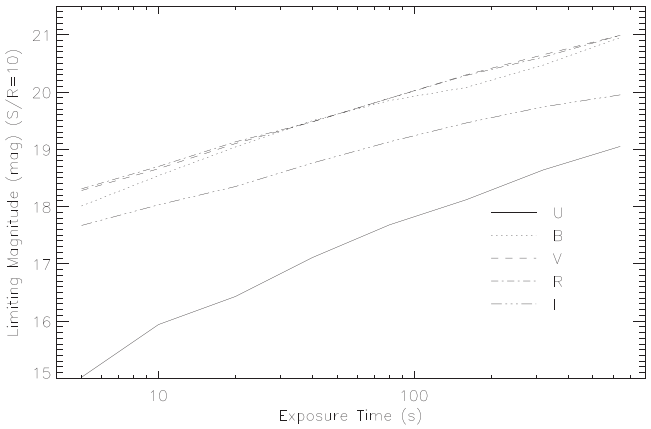

Figure 9. Same as in Figure 8, but for a signal-to-noise ratio of S/N = 10.

The slit and decker assembly is composed of decker, the slit width adjuster, calibration reflector, and driving device. The top surface of the slit is aluminized stainless steel with high reflecting power, while the slit edge was polished to be very sensitive and should not be touched. The slit is tilted by 20° with respect to telescope optical axis, and the projected slit width can be adjusted remotely through the main console in the range of 0.05–1.0 mm (corresponding to 0.″5–10.″6), which is displayed on the main console via the voltage value. The size of the slit jaws is 32.8 mm × 38 mm, and the effective length of the slit is 28.8 mm (corresponding to 5.′1). The slit jaw reflects the light to the guiding system.

There are six positions on the filter wheel for the filters of Clear, Corning 4–71, Schott *BNG*–37, *BG*–39, *GG*–475, and *RG*–695. All the filters have the same size of 25 mm × 25 mm. The central wavelengths of filters could be matched with the first- or second-order of the spectrum by the softwares automatically.

There are three wavelength calibration lamps (Fe-Ne, Fe-Ar, and He-Ar) and a flat-fielding lamp for the calibration device. All of lamps can be controlled remotely. For the Fe-Ne lamp, a standard 1.5-inch ISTC Model #WL-22810 is supplied, and other types of lamps actually can be used as well, such as Hamamatsu and Starna. The maximum working current is 20 mA, and the normal working current is 10–12 mA. The Fe-Ar lamp ISTC Model is #WL-22611. For the safety of He-Ar lamp, the DC power should be used for the supply. As for the flat-fielding lamp, the power is the standard 12 V DC, 1.5A halogen tungsten lamp (Sylvania #808-301550), and it usually can be used for 1000–2000 hours. Meanwhile, there are four condensers for the calibration lamps, which are made of quartz or pyrex glass. The diameters are 25 mm, and the focal lengths are $f = 38$ mm. The field lens is made of quartz, with a diameter of 38 mm and a focal length of 64 mm.

The mirror of the collimator is an off-axis parabolic aluminized reflector, made of pyrex glass. The aperture of the mirror is $D = 110$ mm, and the focal length is $f = 674$ mm. The off-axis angle is 8.1° and the focus can be adjusted remotely.

At present, there are six reflecting blazed gratings mounted on the OMR spectrograph. The gratings are made of aluminized pyrex glass and can be switched manually. The parameters of the blazed gratings are given in Table 4, including the number of the gratings, the grooves, groove areas, reciprocal linear dispersions, dispersions, blaze wavelengths of the first-order spectra, and the blaze angles. The overall working wavelength coverage of the gratings is ∼3700–10000 Å. For the specific grating, the wavelength coverage is adjustable, and it can be estimated through parameters of Table 4 and the size of the CCD. For instance, the wavelength coverage of gratings of 1200 lines/mm is ∼1380 Å, while for the grating of 300 line/mm, it is ∼5420 Å. The SPEC software, which is the camera-controlling software designed and installed with the PI Spec-10 CCD camera, can recognize the gratings, and the wavelength coverage can be adjusted via SPEC according to the requirements of the observers.

The camera is a Schmidt-Cassegrain system. The useful aperture is $D = 100$ mm, and the focal length is $f = 150$ mm. The CCD mounted is a PI Spec-10 PIXIS 1340 × 400 scientific CCD detector, which delivers the highest sensitivity possible and >16–bit dynamic range for spectroscopy applications. The pixel size is 20 × 20 μm pixels, and the CCD size is 26.8 × 8.0 mm^2. The deepest cooling temperature is −75° C. The QE of the CCD is shown in Figure 12, which is midband.

The guiding system of the OMR is composed of a reflecting system and a CCD Camera. In the reflecting system, the slit reflecting mirror is aluminized and the rms of the surface flatness is 1/4 λ. For the transfer lens, the diameter is 50 mm, with a focal length of $f = 260$ mm. While for the focal lens, the diameter is 36 mm, with a focal length of $f = 85$ mm. Both of the lenses have been coated. The CCD camera is an Alta U42 CCD, made by Apogee Imaging Systems, Inc. The sensor is E2V CCD42–40, and the size is 2048 × 2048 pixels. The Gain is 1.3 e$^-$ count^{-1} and the maximum digitized well capacity is 82 k e$^-$. The dark current is 0.39 e$^-$ pixel^{-1} s^{-1}.

Similarly, the Landolt standard star Feige 66 was observed with two blazing gratings 1200B and 1200R of the OMR instrument and the total efficiencies (including the atmosphere extinction, the reflecting rate of mirrors, QE of CCD, etc.) have been computed through Equation (1). As described above, the central wavelength and coverage is adjustable; Figure 13 shows the total efficiencies of two gratings 1200B and 1200R, in two different central wavelength and wavelength coverages. It can be seen that the efficiency ranges from ∼1% to ∼2%, which is relatively lower than that of the BFOSC gratings.

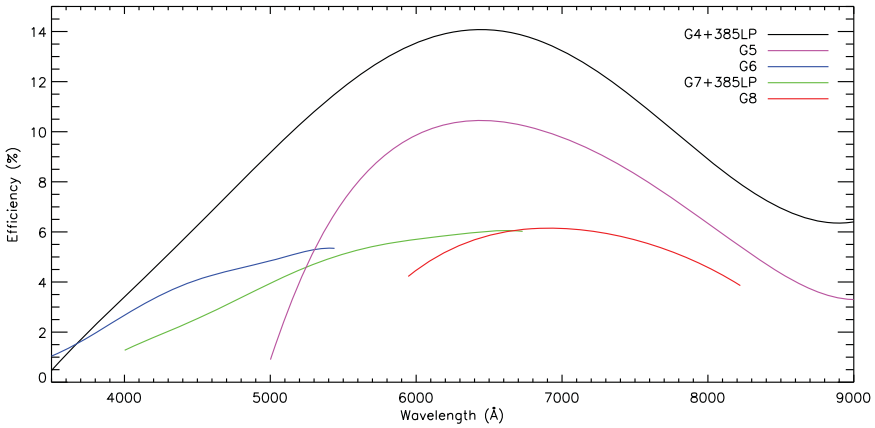

Figure 10. Total efficiencies estimated for grisms G4, G5, G6, G7, and G8 of the BFOSC instrument.
(A color version of this figure is available in the online journal.)

Typically, for a star of $V = 17.3$ mag in an exposure time of 1800s, the signal-to-noise ratio is S/N = 12 at wavelength of $\lambda = 5500$ Å; for a star of SDSS $g = 19.8$ mag in an exposure time of 3600 s, the signal-to-noise ratio is S/N = 5 on average for the whole band.

3.3. The Fiber-fed High Resolution Spectrograph (HRS)

Previously, an echelle spectrograph was mounted on the Coudé focus of the telescope for high-resolution spectroscopic observations. The special design of the optical system is to allow the Cassegrain system and the Coudé system to share the same secondary mirror and there is a relay mirror in the Coudé system. When switching between the two systems, the Coudé system can eliminate spherical aberration and coma aberration sufficiently just by slightly moving the secondary mirror (Su et al. 1989). The resolution power was between R = 16,000 and 170,000 (79 gr mm^{-1}) in the blue beam from 330 nm to 580 nm and R = 13,000 and 170,000 (31.6 gr mm^{-1}) in the red beam from 520 nm to 1100 nm. For an exposure time of 1 hour, the limiting magnitude could reach $V = 9.5$ in the red band and $V = 7.2$ mag in the blue band with a signal-to-noise ratio S/N = 100 (please see Zhao et al. 2000; Zhao & Li 2001).

Since 2010, a new fiber-fed High Resolution Spectrograph (HRS) has been developed by the Nanjing Institute of Astronomical Optics & Technology (NIAOT) to satisfy the scientific requirement of, for instance, exoplanet surveys, the study of stellar abundances, and stellar magnetic activities. The optical layout and light path are shown in Figure 14. The HRS system is available for the Cassegrain focus and composed of four parts: 1) the Cassegrain connector of the telescope; 2) the fiber connector and the micro-optical module for focal ratio changing; 3) the main body of the spectrograph; 4) the data-collecting part of the CCD camera.

The fiber-fed HRS observing mode could be switched to other instruments (such as BFOSC or OMR) conveniently through the Cassegrain focal interface of the telescope within only a few minutes. The calibration system of HRS, the I_2 cell and its heating system, as well as the tip/tilt system are mounted on the interface of the spectrograph. The whole main body is sealed in a protective box and the temperature variation is less than rms = 0.5°C for a week. At present, a 2.″4 aperture fiber is configured and the tip/tilt system is working to improve the efficiency of the system when the seeing is ideal. The fiber of 1.″6 is at the commissioning stage and it could be available very soon. An environmental controlling system can accurately keep the stability of both temperature and humidity for the HRS system. Furthermore, a sub-controlling system of pressure will be installed at this system in the future.

The basic parameters of HRS are listed in Table 5. The working wavelength coverage is 360–1000 nm, and the instrumental efficiency of the spectrograph is $\geqslant$34% for the peak at a wavelength coverage of 640–790 nm (*RI* band), and $\geqslant$10% for $\lambda > 4500$ Å (the whole working band), based on the tests of 2010 November 23. The spectral resolution is 32,000–106,000 for the spectrograph, and it is $R = 49{,}800$ at a fixed slit width of 0.19 mm (corresponding to 1.″8) based on the test of 2011 April 12. The stability of the instrument for the velocity measurement is rms = $\pm$6 m s^{-1}, and the temperature is quite stable even for two weeks. The CCD camera is a back-illuminated first-order red-sensitive E2V CCD 203-82. The size is 4096 × 4096 pixels with a pixel size of 12 μm. The typical QE of the CCD is >90% under the temperature of −100°C in the wavelength coverage of ~500–650 nm, which is shown as the solid line in Figure 15.

The liquid nitrogen (LN) holding time of the system is ~20 hours, and the cooling temperature is −106°C. For *Gain* = 1.01 e$^-$/ADU, the readout noise (RON) is 2.84 e$^-$ at the readout speed of 50 k, 4.29 e$^-$ at readout speed of 100 k,

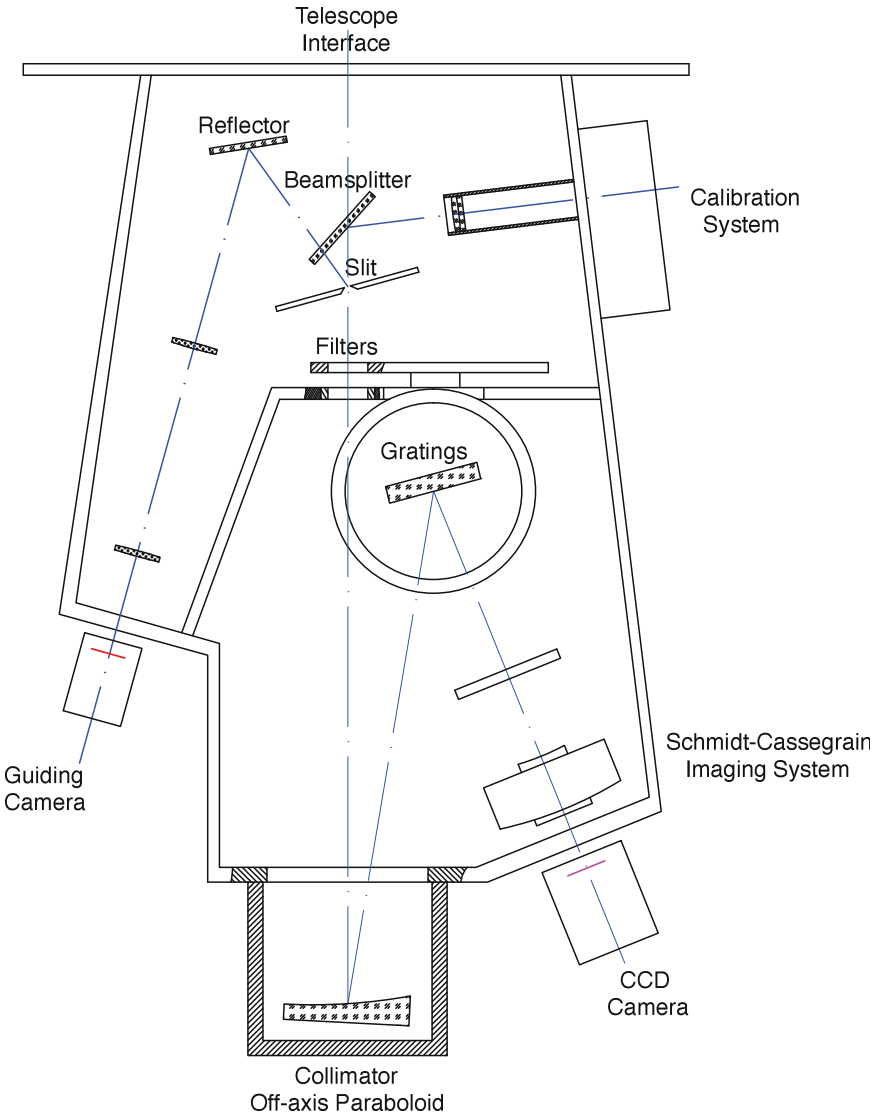

Figure 11. Optical layout of the OMR spectrograph.
(A color version of this figure is available in the online journal.)

and 7.88 e^- at readout speed of 200 k. The distance between the nearby orders of the spectrum is $\geqslant$20 pixels, and the two fibers (2.″4 aperture one and 1.″6 aperture one) can work at the same time. The aperture of the fiber is 100 μm (2.″4), and the fiber length is ∼19 m. The FOV for the guiding camera is $3' \times 3'$, and in the guiding plate the aperture of pupil is 4.″0 in front of the fiber. The temperature variation of the system is rms $= \pm 0.05$°C for a whole night and rms $= \pm 0.34$°C for a week. The tip/tilt system is working normally on the Cassegrain focus. The system, including the astro-frequence comb instrument, is currently in its commissioning phase, and its radial velocity precision dose not yet reach its design goal of a few ∼cm s^{-1}. It is expected that this goal will be achieved once commissioning is complete.

The guiding CCD camera is a GC1380, and the software *AVTUniCamViewer* is used for CCD controlling, exposure time configuration, and data collection. The telescope controlling software can monitor the guiding uncertainty of the guiding system.

An astro-frequency comb calibration system (Zhao et al. 2014, 2015), which is developed by Peking University (PKU), also was installed and is being tested on the 2.16-m telescope. The full spectral wavelength range of the astro-frequency comb is 160 nm and the central wavelength is 640 $\pm$ 20 nm. The observed spacing of the comb teeth is 29.01 GHz. Once working normally, it can greatly improve the measuring accuracy of the stellar radial velocity. The system has significant advantages over the I_2 cell (Wilken et al. 2010). It

Table 4
The Current Parameters of the OMR Gratings

No.	Grooves (l mm^{-1})	Gro. Area (mm)	Rec. Lin. Disp. (Å mm^{-1})	Disp. (Å pix^{-1})	Blz. Wav. (1st order) (Å)	Blz. Ang. (°)
1	150	90 × 90	400	8.0	5000	2.2
2	300	90 × 90	200	4.0	8000	6.5
3	600	102 × 102	100	2.0	6500	11.3
4	1200	102 × 102	50	1.0	8000	28.7
5	300	102 × 102	200	4.0	4224	3.6
6	1200	102 × 102	50	1.0	4000	13.9

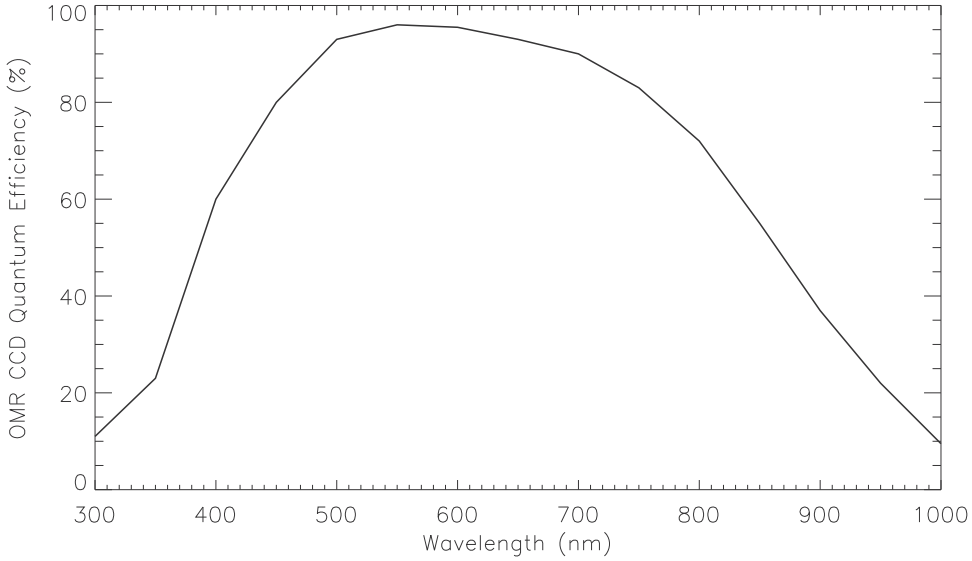

Figure 12. Quantum efficiency of the CCD camera of the OMR Spec-10, which is midband.

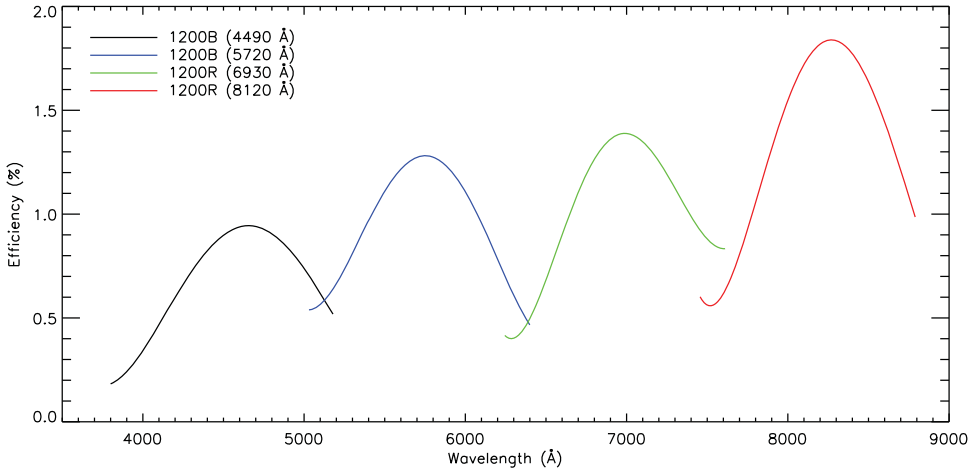

Figure 13. Total efficiency estimates with blazing gratings 1200B/1200R of the OMR, in two different central wavelengths and wavelength coverages. (A color version of this figure is available in the online journal.)

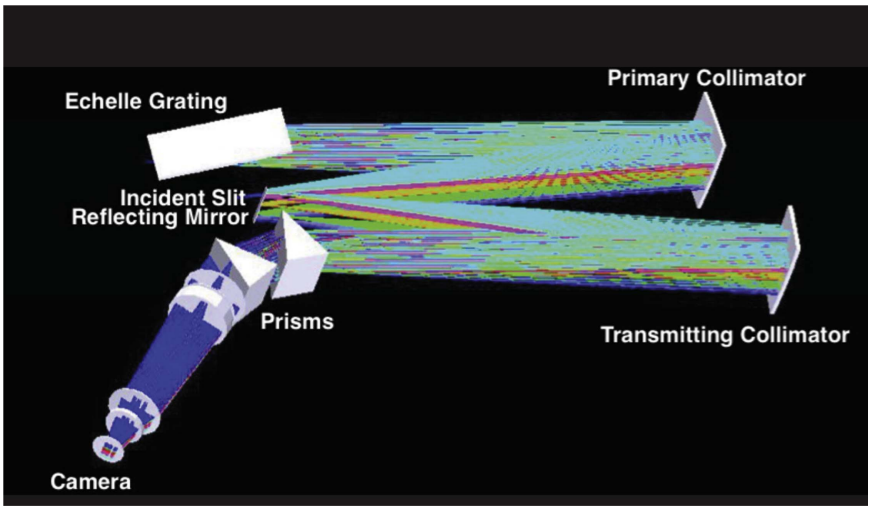

Figure 14. Optical layout and the light path of the fiber-fed HRS spectrograph. (A color version of this figure is available in the online journal.)

Table 5
The Current Instrumental Parameters of the HRS

Tech. Index	Parameters	Notes
Wave. Cov.	3650–10,000 Å	ThAr lamp
Aper. of Fiber	$2\farcs4/1\farcs6$	
Spec. Res.	32,000–106,000	tested on 2011 Apr 12
Stab. of Inst.	± 6 m s^{-1}	Zhao et al. 2014
Effi.	34% at peak value $\geqslant$10% for $\lambda > 4500$ Å	tested on 2010 Nov 23
CCD Camera	E2V 4k × 4k 12 μm Scientific chip, class 1 On-chip Binning 50–200 KHz LN holding time: 20 hours (w/LN auto-filling) LN cooling	2 × 1 binning mode suggested
FOV of Guid. Cam.	$3\farcm3 \times 3\farcm3$	
Temp. var./day	$\pm 0\fdg05$	
Temp. var./week	$\pm 0\fdg34$	

consists of a series of discrete, equally spaced spectral lines with equal intensity, and it is repeatable in a long timescale. Right now, the system has been set up, and the first spectrum simultaneously from the comb and the flat-fielding lamp has been obtained during the engineering run. Meanwhile, a 25 GHz AstroComb Optical Frequency calibration system manufactured by the MenloSystems company, also has been installed on the HRS instrument system recently. The spectral coverage is ~450–720 nm, with the central wavelength of 540 ± 30 nm. The flatness of the spectrum is rms < 5 dB, and the observed spacing of the comb teeth is 25 GHz. The luminous power of the system for the full spectral wavelength range is >10 μW. The two new calibration systems are at the commissioning stage. The two new systems are supposed to be applied in the end of this year.

In order to estimate the total efficiency (including the atmospheric extinctions and reflectivity of the primary/secondary mirrors, among others), a number of standard stars were observed with HRS on 2015 June 30. By using Equation (1), the final result shows that it is >2% at 5500 Å.

In addition, the limiting magnitudes are estimated. Figure 16 is a plot of the signal-to-noise ratio (S/N) at $\lambda = 5500$ Å as a function of exposure time for the stars from $V = 5$ mag to $V = 9$ mag for the HRS system, based on the observing data. For a $V = 9$ mag star, the typical signal-to-noise ratio S/N = 100 for an exposure time of 3000–3600 s. A few observing tests give the S/N in the typical observing conditions of 2012, for a star of $V = 8.85$ mag with an exposure time of 3600 s, the signal-to-noise ratio is S/N = 80 at wavelength of $\lambda = 6000$ Å, and for a star of $V = 7.83$ mag in 2400 s exposure, the signal-to-noise ratio is S/N = 150 at wavelength of $\lambda = 6000$ Å (provided by Xiaoling Yang and Yuqin Chen).

4. Scientific Projects

Since 1989, when the 2.16-m telescope saw its first light, a great many scientific research projects have been carried out in various fields, including: the study of nearby galaxies (star formation rates, gas, and dust content), AGNs and their supermassive black holes (SMBHs), quasars, stellar parameter determinations, exoplanets, supernovae (SNe), gamma-ray

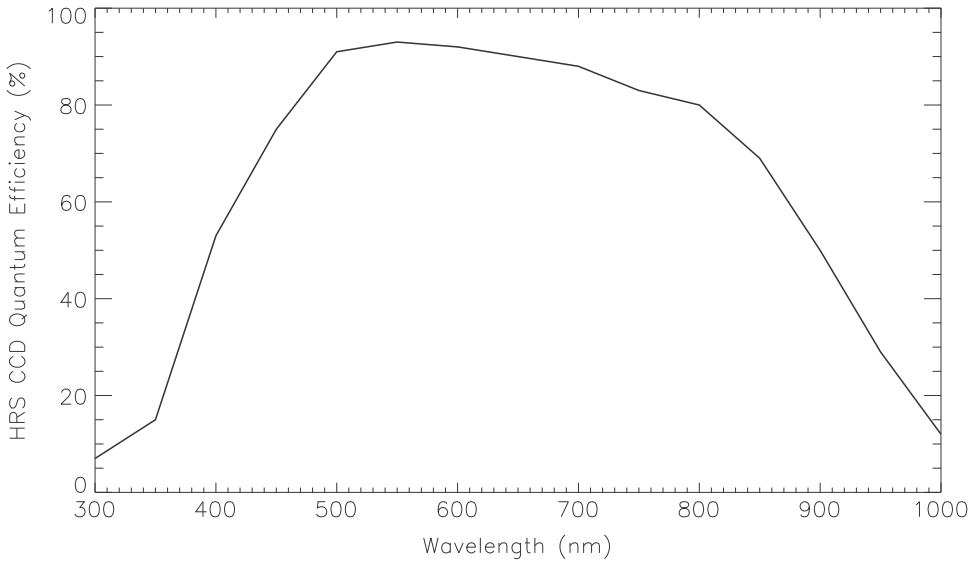

Figure 15. Quantum efficiency of the basic midband CCD camera used on the HRS at −100°C, which is shown by the solid line.

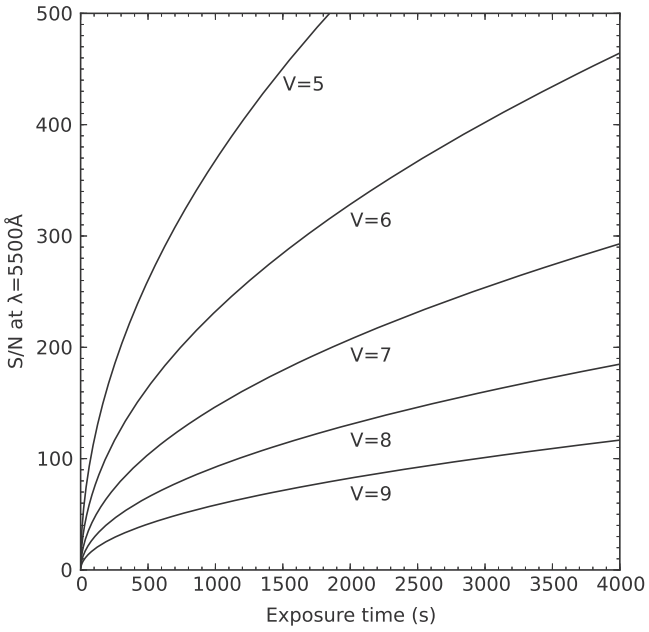

Figure 16. Signal-to-noise ratio at $\lambda = 5500$ Å as a function of exposure time for stars from $V = 5$ mag to $V = 9$ mag by using the fiber-fed HRS spectrograph.

bursts (GRBs), and follow-ups of tidal disruption events. When LAMOST was built, the 2.16-m telescope was also used for the LAMOST follow-up and stellar library observations.

Some of the scientific highlights obtained with the 2.16-m telescope are as follows. In 1993, Wang & Hu (1994) observed the spectra of supernova 1993J with the 2.16-m telescope and found the blueshifted oxygen lines only four months after the optical discovery of the supernova, which is different from the case of 1987A. Approximately 100 G-type giant stars of $V \sim 6$ mag have been monitored with the Coudé HRS system (Zhao & Li 2001). In a joint planet-search program between China and Japan, using the Xinglong 2.16-m telescope and Okayama Astrophysical Observatory (OAO), a number of substellar companions of intermediate-mass giant stars has been discovered by Liu et al. (2008, 2009). Later, a brown dwarf companion candidate was discovered by Wang et al. (2012) and a long-period giant planet has been discovered by Wang et al. (2014), which is actually the first exoplanet discovered jointly with the Subaru telescope, the OAO 1.88-m telescope, and the Xinglong 2.16-m telescope.

In recent years, in order to improve the efficiency of the telescope and to maximize the scientific output, 7–8 key projects with the telescope have been supported for 3–5 years. Each project usually owns ∼20–40 nights per year, which allows us to carry out long-term observations and large-sample surveys. For instance, a number of quasars at intermediate redshift $2.2 < z < 3$ have been identified by Wu et al. (2011, 2013). An Hα imaging survey of ∼1400 nearby ALFALFA galaxies is carried out to study the star formation rate and the stellar distributions. From 1997 to 2002, the spectra of ∼100 blue compact galaxies (BCGs), which was the largest sample before SDSS, have been observed with the 2.16-m telescope, and the metallicity, extinction of dust, and star formation rate of the sample galaxies have been derived by Kong & Cheng (2002), Kong et al. (2002), Kong (2004), Shi et al. (2005), and Kong et al. (2002). A group from Peking University has discovered a high-redshift quasar ($z = 5.06$), J2202+1509, in 2014 November with the 2.16-m telescope, which is SDSS $i = 18.79$ mag (Wang et al. 2016). The redshift is derived from the emission lines, such as Lyα at a wavelength of 1216 Å and

Nv at a wavelength of 1240 Å. This demonstrates that the 2.16-m telescope is able to be used to discover and study high-redshift quasars.

5. Observing Time Application

Each year, the call for proposals begins around 20 October for the period of one month. Astronomers who are willing to use the telescope can submit proposals through the website http://astrocloud.china-vo.org before the deadline. After that, the proposals will be collected and reviewed by the Time Allocation Committee (TAC) of the 2.16-m telescope. The probability of observing nights obtained for observers highly depends on the mark ranking. The target-of-opportunity (ToO) follow-up observations, like transient SNe and GRBs, is supported, which are allowed to be applied and observed when the transient sources happen. The turnaround time (i.e., the time interval between a ToO alert and the start of the first observation) of the 2.16-m telescope depends on the system and configuration being used when it happens. It concludes with the following parts: the readout time of the last frame (∼30–50 s); the time for changing the grisms and adjusting slit width and sometimes it takes even longer when the grism is not on the spectragraph (∼5–10 minutes), the pointing time of the telescope (∼1–5 minutes), the possible time for changing instrument and focusing (∼5–10 minutes), etc. Therefore, it takes ∼10–30 minutes in all for starting the ToO observations.

Since the first light of the 2.16-m telescope, there are astronomers from France, Japan, Taiwan, Hong Kong, etc., beyond China Mainland, applied and used the telescope and publish papers. Until now, there are more than 150 SCI papers published with the data obtained with the 2.16-m telescope since the first light. All these papers have been peer-reviewed, and most of them were published on the high-impact magazines in astrophysics, e.g., *ApJ*, *AJ*, *MNRAS*, and *A&A*, and the impact factors are around ∼4–6, including the articles published in *Nature*. When the key projects are concluded, there will be numerous high-impact articles published in the future.

6. Summary and Discussion

As a 2-m-class optical astronomical telescope in China, the 2.16-m telescope of Xinglong Observatory of NAOC plays an important role in observational astronomy today. There are currently three primary instruments, the BFOSC, OMR, and the fiber-fed HRS, available for the telescope users. When the 2.16-m telescope saw the first light in 1989, various scientific projects were carried out, based on observations of the telescope in the research areas of nearby galaxies, AGNs, supernovae, GRBs, exoplanets, Galactic stars, time-domain astronomy, and many other sciences. Since the LAMOST spectroscopic survey started, the 2.16-m telescope has also been used for the LAMOST follow-ups, in order to identify interesting objects, and for stellar library observations. A great many remarkable studies have been done with the telescope, including the spectroscopic research of the supernova 1993J (Wang & Hu 1994). In recent years, in order to improve the utilizing efficiency of the telescope and the scientific output further, 7–8 key observing projects have been set up, in which the observers own 20–40 nights/year to carry our long-term observations and serial research.

In the future, a number of potential new instruments will be available to the 2.16-m telescope users to improve its observing abilities further, such as an imaging photopolarimeter *RoboPol* (see King et al. 2014), a prototype of which is currently in use at the 1.3-m telescope of the Skinakas Observatory in Crete, Greece, where it works well. A similar photopolarimeter will probably be installed at the 2.16-m telescope in the next one or two years, which will be the first astronomical photopolarimeter in China. It could be used for polarization measurements, for instance, of Seyfert galaxies, blazars, and GRBs. Further, an intermediate-resolution spectrograph (IRS) is being investigated. If it is installed and committed in the future, the projects of intermediate-resolution spectroscopic observations (e.g., X-ray binaries, bright stars, nearby galaxies, and a large number of fainter Galactic stars) could be carried out. In addition, the testing of the astro-frequency comb calibration system is at the commissioning stage. When it is finished, the precision of the radial velocity measurements of Galactic stars could be improved greatly, even to a few $\mathrm{cm\,s^{-1}}$. Recently, a number of adaptive optics experiments were performed on the 2.16-m telescope by engineers from various Chinese institutes, which can improve the spatial resolution and signal-to-noise ratio of targets to a large extent. The exoplanet detection technology group from the Nanjing Institute of Astronomical Optics & Technology, NAOC, and the California State University, Northridge collaborated and built the High Performance Portable Adaptive Optics (HPAO), which is mounted on the Coudé focus of a 2.16-m telescope and succeeded after the testing observations. Although the limiting magnitude of the current HPAO system is faint to 3.8 mag in the *H* band, the system will be upgraded in the next step, and the results can be improved significantly.

This research was supported by the National Natural Science Foundation of China (NFSC) through grants 11003021, 11373003, 11273027, and 11303042 and National Key Basic Research Program of China (973 Program) 2015CB857002. Z. F. acknowledges a Young Researcher Grant of the National Astronomical Observatories, Chinese Academy of Sciences. We thank Yuqin Chen, Liang Wang, and Xiaoying Yang for providing the limiting magnitude measurements of the HRS instrument and thank Yingwei Chen for providing the picture of the 2.16-m telescope.

References

Chen, J. S., Fan, X. M., & Tan, X. Y. 1987, AcASn, 28, 303
Cui, X.-Q., Zhao, Y.-H., Chu, Y.-Q., et al. 2012, RAA, 12, 1197
Fan, Y.-F., Bai, J.-M., Zhang, J.-J., et al. 2015, RAA, 15, 918
Huang, L., Wei, J.-Y., Jiang, X.-J., et al. 2015, AR&T, 12, 44
Huang, L., Wu, H., & Li, H. B. 2012, BFOSC (Beijing Faint Object Spectrograph and Camera) Operating Manual, April
King, O. G., Blinov, D., Ramaprakash, A. N., et al. 2014, MNRAS, 442, 1706
Kong, X., & Cheng, F. Z. 2002, A&A, 389, 845
Kong, X., Cheng, F. Z., Weiss, A., et al. 2002, A&A, 396, 503
Kong, X. 2004, A&A, 425, 417
Li, D.-P. 2001, Opt. Instrum., 23, 2
Liu, Y.-J., Sato, B., Zhao, G., et al. 2008, ApJ, 672, 553
Liu, Y.-J., Sato, B., Zhao, G., & Ando, H. 2009, RAA, 9, 1
Shi, F., Kong, X., Li, C., & Cheng, F.-Z. 2005, A&A, 437, 849
Su, D.-Q., Zhou, B.-F., & Yu, X.-M. 1989, ScChA, 11, 1187
Wang, L., Sato, B., Omiya, M., et al. 2014, PASJ, 66, 118
Wang, L., Sato, B., Zhao, G., et al. 2012, RAA, 12, 84
Wang, L.-F., & Hu, J.-Y. 1994, Natur, 369, 380
Wang, F.-G., Wu, X.-B., Fan, X., et al. 2016, ApJ, 819, 24
Wilken, T., Lovis, C., Manescau, A., et al. 2010, MNRAS, 405, 16
Wu, X.-B., Wang, R., Schmidt, K. B., et al. 2011, AJ, 142, 78
Wu, X.-B., Zuo, W.-W., Yang, J.-Y., Yang, Q., & Wang, F.-G. 2013, AJ, 146, 100
Zhang, J.-C., Ge., L., Lu, X.-M., et al. 2015, PASP, 127, 1292
Zhao, G., & Li, H.-B. 2001, ChJAA, 1, 555
Zhao, G., Qiu, H.-M., Chen, Y.-Q., & Li, Z.-W. 2000, ApJS, 126, 461
Zhao, F., Wang, H., Zhao, G., et al. 2015, AR&T, 12, 1
Zhao, F., Zhao, G., Lo Curto, G., et al. 2014, RAA, 14, 1037
Zheng, W.-K., Qiu, Y.-L., Wang, J., et al. 2009, AR&T, 6, 2
Zhou, Z.-M., Wu, H., Huang, L., et al. 2014, RAA, 14, 1393